# Synchrotron x-ray study of the structures and phase transitions of monolayer xenon on single-crystal graphite

Hawoong Hong, C. J. Peters, A. Mak, and R. J. Birgeneau
*Department of Physics, Massachusetts Institute of Technology, Cambridge, Massachusetts 02139*

P. M. Horn
*IBM Thomas J. Watson Research Center, Yorktown Heights, New York 10598*

H. Suematsu
*Department of Physics, University of Tokyo, Bunkyo-ku, Tokyo 113 Japan*
(Received 21 February 1989)

The phases and phase transitions of solid xenon monolayers on a graphite single crystal were investigated using high-resolution synchrotron x-ray scattering. As the temperature is lowered a sequence of incommensurate solid phases (aligned→rotated→reentrant aligned) occurs. This sequence is followed by an incommensurate-commensurate transition. Zero-temperature mean-field theories are able to explain the C-IC transition but not the reentrant rotational transitions. The corrugation of the adsorption potential and the width of domain walls are estimated using relaxation simulations at zero temperature.

## I. INTRODUCTION

In nature, there are many physical systems whose phases are governed by two competing interactions or periodicities.[1] Among these are solids with charge-density waves,[2] adsorbed monolayers,[3] and modulated magnetic systems.[4] Perhaps the most thoroughly studied competing interaction system is that of the monolayers of rare gases adsorbed onto a graphite surface.[3] These systems are especially attractive for a number of reasons. (i) The interactions between constituent atoms are simple and well known. (ii) There are novel features of the physics which are unique to two dimensions. (iii) The two-dimensional nature of the system makes numerical calculations on large systems tractable. (iv) The high anisotropy of the binding energy of graphite allows one to study an atomically smooth surface of a macroscopic size without much difficulty. (v) The basal plane of graphite is very inert to contamination, so the surface can be easily cleaned.

In spite of the extensive work done on the rare gas on graphite system many questions remain unanswered and new developments continue to occur. For example, renormalization-group calculations have produced finite-temperature phase diagrams,[5,6] computer simulations with realistic models have provided detailed information about energetics of the phases and defects,[7,8] and experimental controversy about the nature of the phases and the order of the phase transitions remains.

We have investigated xenon monolayers on a graphite basal surface. A series of experiments has been performed using synchrotron x-ray scattering as a probe of adsorbed layers on single-crystal graphite substrates.[9] The experimental configuration allows for much better resolution than previous electron diffraction[10] or x-ray diffraction[11] measurements in the same area of the phase diagram.

The use of crystalline graphite instead of powdered graphite as a substrate automatically provides orientational structural information. Furthermore, we were able to select a graphite crystal which was of unusually high quality so that scans were typically resolution limited. A brief synopsis of part of these results appears elsewhere.[12]

Below its melting temperature, the xenon monolayer goes through a sequence of solid phases. Starting from the high-temperature phase, the xenon monolayer has an incommensurate solid aligned with respect to a substrate axis, an incommensurate solid rotated from this axis, a realigned incommensurate solid and, finally, the commensurate solid. In the above phases and the transitions between them, domain walls play an important role.

In Sec. II we discuss the relevant theories, most of which begin with the domain-wall limit. We will then present our data in the light of these theories. In the course of this we will try to examine the energetics predicted by computer simulations and other theories. We will clarify some of the results for the commensurate to incommensurate (C-IC) transition which appear to contradict previous results either from this group or others.[10,11] Finally, a speculative explanation for one of the rotational transitions will be given.

## II. THEORY

Although the lateral corrugation of the adsorption potential between the graphite substrate and the rare-gas adatoms is small, this energy is important in deciding what structure the monolayer of rare-gas atoms will have. The periodicity imposed by the substrate potential is usually different from the periodicity favored by an unper-

 

turbed monolayer. For example monolayer Xe and Kr prefer lattice constants (4.38 Å for Xe and 4.00 Å for Kr) which are close to, but different from, that of the $\sqrt{3}\times\sqrt{3}R\,30°$ superlattice (4.26 Å) on a graphite surface.

As the lattice constant of the monolayer approaches that of the commensurate phase, one can imagine that the corrugation in the substrate potential would induce a set of domain walls separating commensurate regions, which are large in extent when compared with the width of the wall. (Some authors use terms like "discommensuration"[13] or "misfit dislocation"[10,14] instead of domain wall.) The C-IC transition then can be regarded as a transition in which the size of the domains tends to infinity. In this treatment, we consider the free energies of the monolayer in terms of the size of the domains.[1]

Let us assume that we have a hexagonal array of domain walls. In the case of a weakly incommensurate phase, the wall energy per unit length and the wall crossing energy ($f_I$) can be assumed to be independent of the size of the domains. In the case of a superlight wall one can calculate the free energy per unit area[15]

$$F=\frac{2}{3\sqrt{3}l^2}\left[\frac{l}{a'}(\zeta_0+\zeta)+2f_I\right], \tag{1}$$

where $l$ is the length of one side of the hexagonal domain. $\zeta$ is the chemical potential, which is added to the free energy because the wall has a xenon areal density which is lower than the commensurate density. The first term is the domain-wall formation energy which is proportional to $1/l$. From dimensional considerations it is evident that the crossing energy ($f_I$) of the walls contributes as $1/l^2$.

In addition to the hexagonal domain wall phase, it is also possible to have a striped phase in which the walls are oriented in one direction. According to this form of mean-field theory, at $T=0$ the sign of the crossing energy determines whether there will be a striped phase and whether the C-IC transition will be first order or continuous.[16] If the sign of $f_I$ is positive, a striped phase will be energetically favored and the C-IC transition will be a continuous one between the striped phase and the commensurate phase. Otherwise, the C-IC transition will be a first-order transition to a hexagonal domain phase.

At a nonzero temperature, the walls should fluctuate. For the striped phase this will cause an effective entropic repulsion between the walls due to wall collisions, adding a $T/l^3$ term to the free energy. For the hexagonal domain system, the collision term can be ignored.

Villain[16] pointed out that a hexagonal array of domain walls has a degeneracy due to the breathing modes because the hexagonal domains can expand or contract without changing the total length of the walls or the numbers of crossings. The number of these modes is $l/\bar{a}$ where $\bar{a}$ is the order of the lattice constant of the monolayer. Therefore the free energy should become

$$F=\frac{2}{3\sqrt{3}l^2}\left[\frac{l}{a'}(\zeta_0+\zeta)+2f_I-T\ln\left[\frac{l}{\bar{a}}\right]\right]+O\left[\frac{l}{l^3}\right]. \tag{2}$$

From the free energy we can obtain the equilibrium value of $l$ by minimizing $F(l)$ with respect to $l$. At the same time the free energy should be negative for the hexagonal incommensurate phase to be stable against the C phase. From Eq. (2), the critical chemical potential is then

$$\zeta_c=-\zeta_0+\frac{a'}{l_c}T, \tag{3}$$

where $L_c=\bar{a}e^{(1+2f_I/T)}$.

One should notice here that for the same chemical potential the free energy of the striped phase (with positive $f_I$) will be positive.

Coppersmith *et al.*[17] suggested that a crystalline array of domain walls as a lattice can be unstable against the creation of dislocations. In this case, the system goes through a "domain wall liquid" (or "reentrant fluid") phase in the course of the transition from the commensurate solid to the incommensurate solid. The stability of the domain wall lattice depends on the behavior of its elastic constants near the C-IC transition. If the domain wall liquid does not exist, then for positive $f_I$ there will be a first-order transition from the hexagonal domain phase to the commensurate phase.

Kardar and his collaborators[5,6,18] investigated rare gases on graphite using real-space renormalization-group techniques. They have been able to produce phase diagrams for the rare-gas layers using a striped helical Potts model for the domain wall network. These phase diagrams match some features of the experimental results quite well. The main predictions of their calculations for krypton layers are that there is a reentrant fluid phase between the C-IC transition, and that at low temperatures there should be a striped incommensurate solid.

The reentrant fluid phase that is associated with the krypton C-IC transition was originally discovered experimentally[19] and has been studied thoroughly since that time. However, the predicted Kr striped phase has not been observed. Recently, Fain and co-workers have reported observation of a striped phase for $D_2$ monolayers on graphite.[20]

Halpin-Healy *et al.*[18] showed that with some specific choices of the microscopic parameters, the xenon layer may have a striped phase, as well, but the reentrant fluid was excluded. In their phase diagram, at constant pressure, the solid xenon monolayer goes through a hexagonal incommensurate (HIC) phase, striped incommensurate phase, commensurate (C) phase, and a bilayer phase. Depending on the strength of corrugation of the surface adsorption potential ($V_0$), we may have bilayer condensation anywhere between the HIC phase and the C phase. The value of $V_0$ varies by as much as a factor of 3 in the literature. In the Halpin-Healy *et al.*[18] calculation, a value of the wall crossing energy ($f_I$) was chosen to give a striped phase in the phase diagram. As the wall crossing energy changes, the region of the striped IC solid can become extremely small. Furthermore, their real-space renormalization-group technique does not include the effect of the breathing modes which tend to stabilize the hexagonal domain wall network at the expense of the striped phase.

Up to this point, both the two-dimensional solid and the domain-wall network have been assumed to be aligned along symmetry axes of the substrate. However, this is an unnecessary restriction. Novaco and McTague[21] have calculated the linear response of a two-dimensional solid to the substrate potential in the harmonic approximation at $T=0$. They showed that an incommensurate monolayer may rotate from the aligned orientation to minimize the strain energy density. This rotation occurs when $c_l \geq \sqrt{2}c_t$. ($c_l$ and $c_t$ are, respectively, the longitudinal and transverse sound velocities of the monolayer.) For a two-dimensional floating solid, which has a Lennard-Jones–type interaction, $c_l=\sqrt{3}c_t$. This relation is called the two-dimensional Cauchy relation. Thus the condition given by Novaco and McTague[21] is satisfied for almost all solids except those very close to the C-IC transition. Villian[22] showed that in the domain-wall limit, a monolayer can be rotated by tilting the walls. In this case, the condition for rotation is $c_l \geq 2c_t$.

Shiba[23,24] accommodated both of the above possibilities. He treated interactions between adatoms as an elastic continuum and added discrete interactions between the monolayer atoms and the substrate. He showed numerically that a monolayer will rotate when the misfit is larger than a certain critical value. This critical misfit is about $0.7/l_0$ for a Cauchy solid. $l_0$ (dimensionless wall-width parameter) is a constant representing the ratio between the interactions of adatom to adatom and adatom to substrate.

The above theories were calculated at zero temperature. For the behavior at a finite temperature, there does not appear to be any thorough theoretical treatment. Some authors[15,25] briefly mention that the rotation can be suppressed by a sudden change of wall direction from $\theta$ to $-\theta$. If this kink occurs many times on a single, long wall, the average rotation angle will be zero. When the distance ($y_b$) between kinks is much longer than the domain size, domain walls will rotate by $\theta$. Consequently the lattice of the adatoms will rotate, too. If $y_b$ is of the order of the size domains, the situation becomes more complicated. In this case, we can imagine that the rotation angle will be reduced and that there could be a thermally induced transition from the aligned phase to the rotated phase.

## III. EXPERIMENTAL TECHNIQUE

The x-ray scattering experiments were carried out at the IBM-MIT beam lines X-20A and C, at the National Synchotron Light Source (NSLS), Brookhaven National Laboratory. A full description of the beam lines can be found elsewhere (Ref. 19, Specht *et al.*). The scattered beam from the sample was detected after being collimated by the Ge(111) analyzer with the scattering plane perpendicular to the floor. The in-plane transverse resolution results from the vertical angular divergence of the beam (0.013° full width). On the beam line X20A, Si(111) crystals were used for the monochromator. Asymmetrically cut Ge(111) crystals were used on X20C. The resulting radial resolutions were 0.000 24 $\text{Å}^{-1}$ (with Si monochromators) and 0.000 32 $\text{Å}^{-1}$ (with asymmetrically cut Ge monochromators) half-width at half maximum (HWHM).

We will now discuss briefly the substrates and the sample cell. We used two different graphite crystals as substrates. The first graphite crystal used was a natural one picked out from a piece of limestone from New York. The second one was a byproduct of steel production (KISH graphite). The samples were about $1\times2\times0.05$ $\text{mm}^3$ in volume with the $c$ axis along the narrow direction. The substrate was held by tantalum tweezers. To heat the substrate a current was passed through the graphite itself in the direction of the $z$ axis. A 5%W95%Re-26%W74%Re thermocouple attached to the tantalum holder near the substrate was used to measure the temperature during the cleaning procedure.

In addition to the single crystal described above, the sample cell contained a mass of vermicular graphite which was prebaked at 600 °C outside of the cell. The chamber holding the vermicular graphite had Be windows on opposite sides. This large surface area ballast ($\sim 10$ $\text{m}^2/\text{g}$) of vermicular graphite was used to control the surface coverage on the single crystal. That is, by keeping the single crystal and the large mass of vermicular graphite at the same chemical potential, the coverage on the single crystal could be controlled. At the end of the experiment, by scattering from the xenon physisorbed on the vermicular graphite we confirmed that the coverages on the single crystal and the vermicular graphite were the same within the errors.

The temperature control was better that $\pm0.01$ K over an hour, while the overall temperature drift was less than 0.1 K per day. A typical scan took less than 1 h. The sample cell, gas handling system, flexible vacuum tube line, and turbomolecular pump were baked overnight to obtain a base pressure of $10^{-7}$ Torr. As we shall discuss below the overall cell was quite clean with the sample surface coverage remaining fixed for times in excess of a week.

To obtain the precise coverage of the xenon atoms on the graphite surface, we measured a Kr isothermal adsorption; this gives a clear signature of the commensurate to incommensurate (C-IC) transition. We defined one monolayer (1 ML) to be the coverage at the onset of the C-IC transition for krypton, that is, at completion of the commensurate phase. This corresponds to point $A_1''$ in Thomy and Duval's designation for the various transition points on an isothermal adsorption curve.[26]

We tested the quality of the graphite surfaces using diffraction from the monolayer Kr commensurate phase. For both single crystals we obtained Kr peaks which were resolution limited in the longitudinal direction. This implies that the graphite surfaces have a coherence length of at least a 1 $\mu$m. We also obtained the in-plane and out-of-plane mosaicity of the graphite single crystal surfaces from the transverse scans of the Kr commensurate phase. During data analysis, each model function was convoluted with the resolution function and the measured mosaicity. We found that the natural graphite crystal had a complicated in-plane mosaic structure. This mosaic gave some difficulties in analyzing data for the transverse scans. Fortunately, the Kish graphite

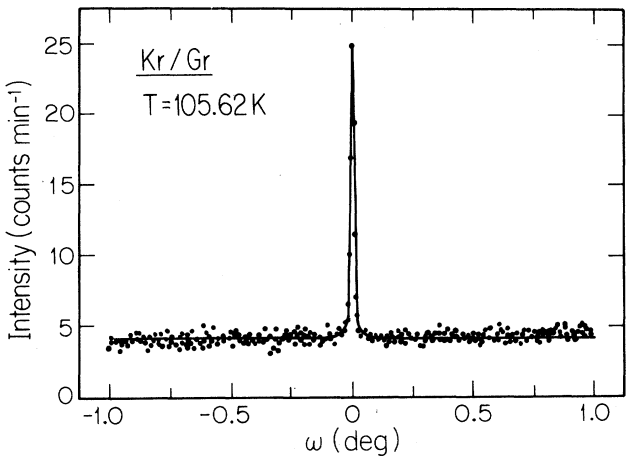


FIG. 1. Transverse scan of commensurate krypton. The commensurate krypton was formed on the KISH single crystal used in the second part of the monolayer study.

crystal showed only one in-plane resolution-limited krypton commensurate peak as shown in Fig. 1.

## IV. EXPERIMENTAL RESULTS

We investigated xenon layers at coverages of $f=0.90$, 0.96, 1.02, and 1.16 ML at low temperatures. The experiment was carried out in a closed-cell configuration so that the actual coverage varied slightly with temperature as the three-dimensional xenon vapor pressure varied. Figure 2(a) shows the sequence of phases investigated in this experiment. The phase at the top of Fig. 2(a) occurs at the highest temperature; proceeding downward, the phases at lower temperatures are shown. Of the various coverages studied, only the 0.90 monolayer (ML) system evolves differently from the others. At 0.90 ML xenon coverage the system has neither the commensurate phase nor the realigned incommensurate phase. At all higher coverages studied, the overall behavior is as depicted in Fig. 2(a). An overall schematic phase diagram excluding the rotational transitions is shown in Fig. 2(b). Representative longitudinal and transverse scans in the different phases for the coverage of $f=1.16$ are shown in Fig. 3.

Let us explain the complicated sequence of phases in detail with the help of Figs. 2 and 3. When the xenon monolayer freezes, immediately below its melting temperature ($T=116\sim134$ K depending on the coverage[27,28]) it forms an incommensurate solid [Fig. 3(a)] whose axes are aligned at 30° relative to those of the graphite surface, that is, along graphite (110). At the freezing temperature, the xenon solid has a wave vector $Q(1,0)=1.59$ Å$^{-1}$. On cooling, as more xenon atoms are adsorbed onto the graphite surface, the density of the solid monolayer increases; in turn, $Q(1,0)$ increases. When the wave vector reaches $Q\simeq1.62$ Å$^{-1}$, the monolayer undergoes a first-order transition to a rotated incommensurate phase [Fig. 3(b)].

At the transition, the rotation angle with respect to the Gr(110) direction jumps discontinuously to ±0.6°. The

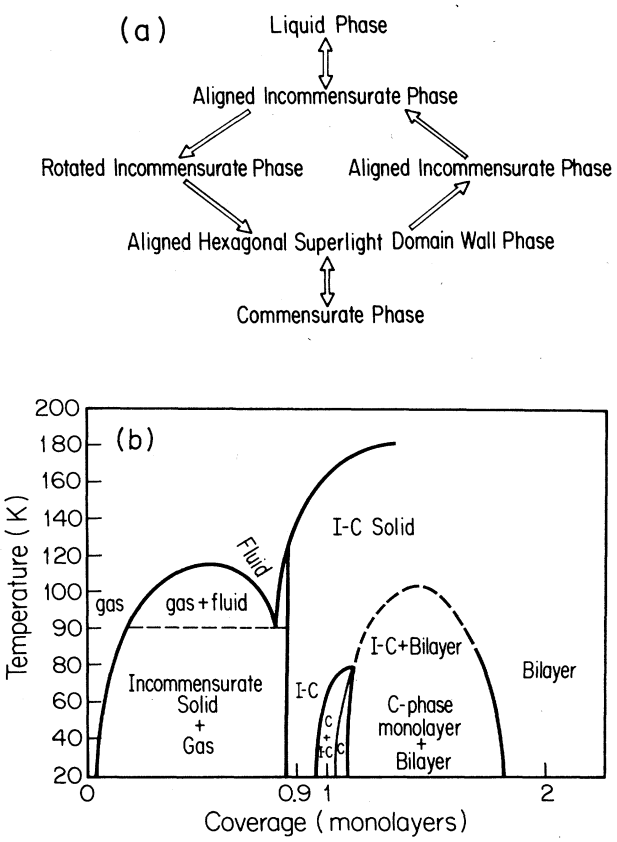


FIG. 2. (a) Phases and phase transitions of xenon on graphite in the monolayer coverage region. A higher location means higher temperature while the arrows indicate the possible transition directions. (b) Schematic phase diagram in the monolayer coverage region. The rotational phase boundaries are not shown explicitly.

rotation angle decreases continuously as the temperature is lowered further. At $Q=1.67$ Å$^{-1}$, the rotation angle goes to zero; then the realigned incommensurate phase [Fig. 3(c)] appears. In this phase we were always able to observe the satellite peaks due to the network of hexagonal domain walls. Around 60–70 K, the xenon layer undergoes another first-order transition from the above realigned incommensurate phase to the $\sqrt{3}\times\sqrt{3}R30°$ commensurate phase [Fig. 3(d)].

On heating, the wave vector $Q(1,0)$ of the xenon layer behaves in exactly the same fashion as in the cooling cycle, including the C-IC transition. However, when we start the heating cycle either from the commensurate or from the realigned incommensurate phase, the xenon layer does not rotate at all. Since the superlight hexagonal domain wall phase is symmetry equivalent to the aligned IC phase, there is only one phase transition, the C-IC transition, in the heating cycle.

### A. Xenon rotation

Plots of rotation angles versus incommensurability ($\epsilon=Q_c-Q$) are shown in Fig. 4 for each coverage. For

each coverage, when the incommensurability is approximately $\epsilon=0.08$ Å$^{-1}$, the rotation angle jumps from zero to $\simeq 0.6°$. This rotation of the monolayer is manifested in the two split peaks in the transverse scan, as in Fig. 3(b). There is, in addition, typically some scattering at the center of the two peaks. These features mean that some patches of the layer rotate clockwise, other patches rotate counterclockwise, and some parts of the layer may remain aligned. As the temperature is lowered, the rotation angle decreases continuously to zero.

For the 0.90 ML xenon layer, $\epsilon$ did not decrease below 0.025 Å$^{-1}$; further, the rotation angle did not go to zero upon cooling. At this coverage, the layer remained rotated even at the lowest temperature ($T=26.80$ K) that was studied. At higher coverages, realignment occurred at $\epsilon\simeq 0.033$ Å$^{-1}$. For the rotated phases, we can fit the rotation angle to a power law. A function $\Theta=a(\epsilon-\epsilon_c)^{1/2}$, as predicted by mean field theory, fits reasonably well for all of the three high coverages although we certainly cannot preclude other functional forms. These power laws are shown as bold curves in Fig. 4. The critical incommensurability $\epsilon_c$ is 0.033 Å$^{-1}$. If we identify this point as the critical misfit $0.7l_0$ predicted by Shiba,[23,24] we obtain 36 for $l_0$. This value will be compared later with $l_0$ estimated in other ways.

The fact that the xenon layers start to rotate at a finite misfit with a rotational angle increasing continuously with the misfit is in qualitative agreement with Shiba's predictions.[23,24] However, the rotation angle is much smaller that predicted. At a high incommensurability Shiba's theory asymptotically approaches the first-order approximation in the weak potential limit.[21] In this limit, the rotation angle is given by

$$\theta=m(1-2c_t^2/c_l^2)^{1/2}\ , \tag{4}$$

where $m$ is the relative misfit $(Q_c-Q)/Q$. For a Cauchy solid, the monolayer will be rotated by $\theta=m/\sqrt{3}$. At $\epsilon=0.08$ Å$^{-1}$ this approximation predicts a rotation of the layer by 1.6°, which is substantially larger than the observed rotation.

The reduced rotation angles and the additional transition from the rotated to the nonrotated phase at high temperature and high misfit must be finite-temperature effects. The orientational fluctuation of domain walls or the excitation of transverse phonon modes which are related to the rotation can reduce the rotation angle or quench the rotation completely. Simple symmetry arguments would suggest that this transition is in the two-

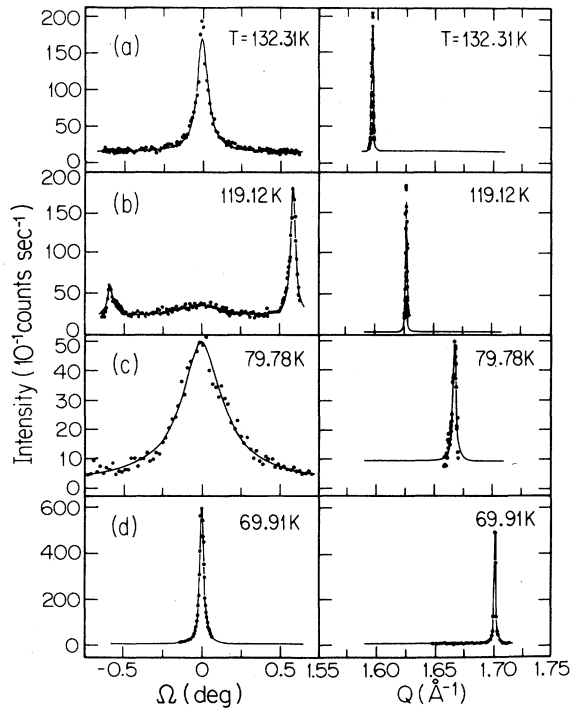


FIG. 3. Representative angular and radial scans for $f=1.16$ layers of xenon on graphite. The intensity is normalized to that obtained for a storage ring current of 100 mA.

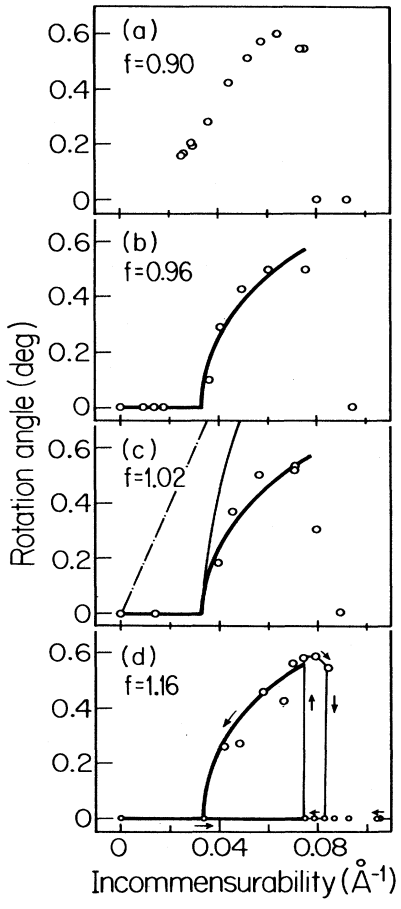


FIG. 4. Rotation angle vs incommensurability. The bold curve is the $\frac{1}{2}$ power law described in the text. In (c) the light solid curve is Shiba's prediction while the dashed line is the lowest-order Novaco-McTague approximation. In (d) the path of the temperature cycle is indicated by arrows.

dimensional Ising universality class.[15] In the present case, however, it is not clear why the transition is first order.

Ar (Ref. 29) and Kr (Ref. 30) monolayers also exhibit rotated phases. The rotation angle and the incommensurability at the onset of rotation for Ar and Kr layers follow Shiba's prediction for the Cauchy solid quite well. Thus there is no evidence for these systems for the finite temperature effects discussed above.

We observed a large hysteresis in the two rotational transitions. The arrows in the plot in Fig. 4(d) show the experimental paths taken. In the rotational transition at high temperature, the hysteresis was as wide as 0.01 $\text{Å}^{-1}$. When we raised the temperature starting from the aligned incommensurate phase to the rotated phase region, the layer did not rotate at all, that is, in the heating cycle, there was no rotational transition. We presume that the absence of the rotated phase in the heating cycle is due to the immobility of the domain walls.

### B. Commensurate to incommensurate transition

Figure 5 shows the evolution of the incommensurabilities with temperature. As noted previously, for a coverage of 0.90 ML the xenon remains incommensurate with respect to the graphite at all temperatures. As the coverage is increased a C-IC transition occurs with a temperature ($T_{\text{C-IC}}$) which increases with increasing coverage. The $T_{\text{C-IC}}$'s) were ~55, 70, and 73 K for the coverages of 0.96, 1.02, and 1.16 ML, respectively.

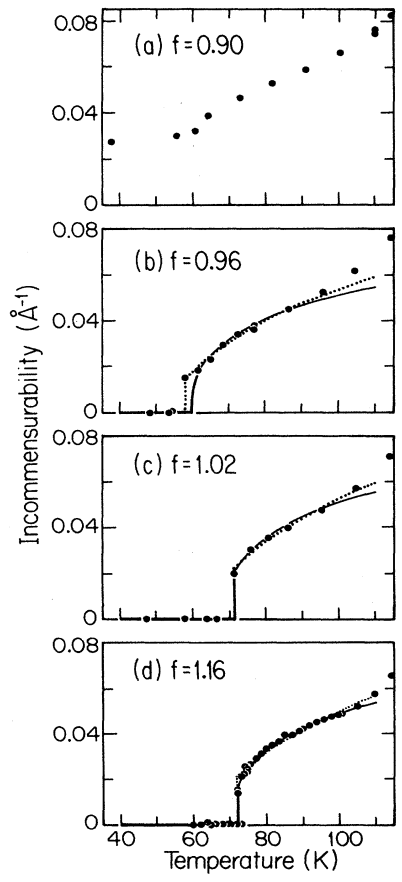


FIG. 5. Incommensurability vs temperature. The solid lines are the results of best fits to single power laws with $\beta=\frac{1}{3}$ while the dotted lines are the power law with $\beta=\frac{1}{2}$.

There has been a number of previous studies of the C-IC transition of the xenon monolayer system. Using transmission high-energy electron diffraction (THEED), Venables and his co-workers[10,31] studied monolayer and bilayer xenon on graphite. As is usual in electron diffraction, these experiments used a single crystal. In the early experiments, neither the surface coverage near the actual pressure was held constant; rather, the measurements involved fixed impinging rates of xenon atoms, which were represented by effective pressures at room temperature. In the most recent experiments (Ref. 31, Hamichi *et al.*) the pressure is indeed held fixed; the pressure is typically in the $10^{-8}$–$10^{-5}$ Torr range while the temperature is varied between 80 and 50 K. In such temperature sweeps, the coverage varies drastically with temperature. This contrasts with our technique where over the same temperature range the coverage is essentially constant. Further, in the THEED experiments the measurement time is 10 sec and the cooling rate typically $\leq 0.5$ K/min. This constrasts with scan times of 2–30 min and equilibration times of up to 2 h in our synchrotron x-ray measurements. Given these differences, the general agreement between the two experiments is quite good. We will comment on the apparent discrepancies below.

Finally, Mowforth *et al.*[32] speculated from their powder x-ray data that a sequence of locked phases exists before the layer reaches the commensurate phase. These locked phases have rotated domains. Even with our much higher resolution data from excellent single crystal substrates, we did not observe any indication of nonzero jumps in lattice constant in the incommensurate phase.

The layer with xenon coverage $f=1.16$ was studied most extensively. The C-IC transition in this coverage showed a clear first-order transition at ~72.8 K. By raising the temperature in 0.5-K steps, we observed a sequence of scans partly shown in Fig. 6. At 71.86 K, there was only a commensurate peak. An incommensurate peak emerged at 72.83 K, but the commensurate peak still existed, albeit with an amplitude which varied with time for periods in excess of 1 h. By 73.18 K the commensurate peak disappeared completely. Though the transition is first order, the continuous part of the $\epsilon$ versus $T$ curve is well described by a power law.[33–35] We included only the data below 100 K, where a good fit to the form $A[(T/T_0)-1]^{\beta}$ was obtained with parameters $A=0.065\pm0.002$, $\beta=0.33\pm0.08$, and $T_0=70.9\pm01.8$ K. The solid line in Fig. 5(d) indicates this curve. The data were also fit to a power law with $\beta$ held fixed at 0.5; this is shown as a dotted line in Fig. 5(d). The $\beta=0.5$ curve generally describes the $f=1.16$ ML data less well especially close to the transition.

As the C-IC transition is approached from the incommensurate phase, the longitudinal widths broaden. The widths are shown in Fig. 8 where we plot the half-width $\kappa$

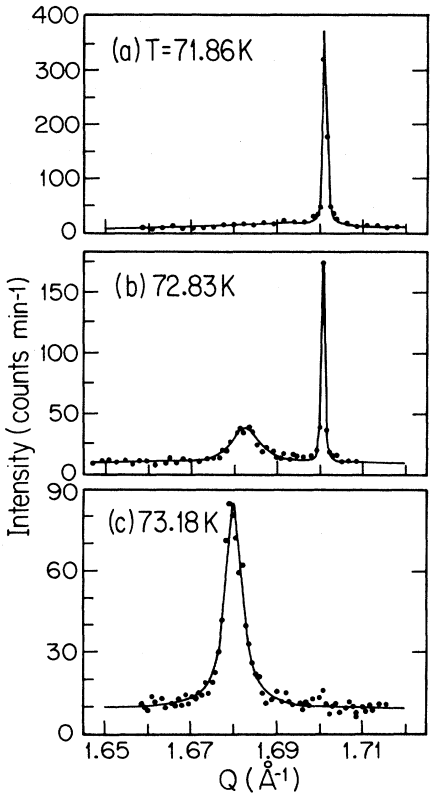


FIG. 6. Longitudinal scans for $f=1.16$ layers of xenon in the vicinity of the C-IC transition.

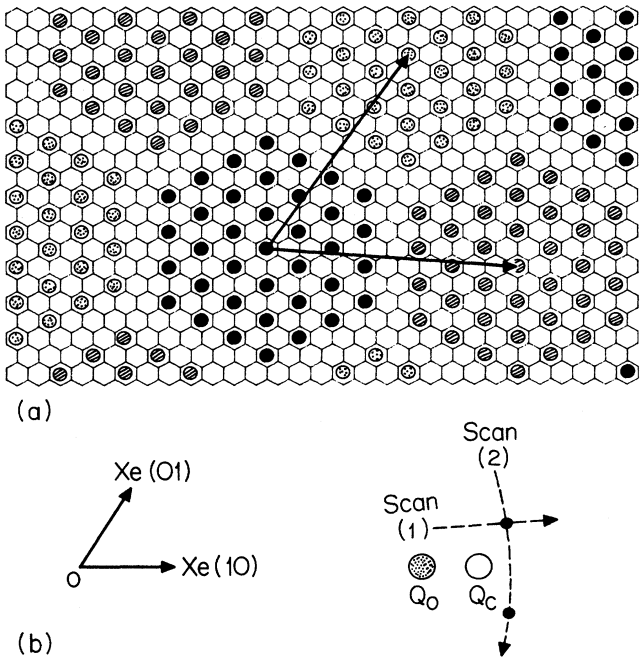


FIG. 7. Hexagonal superlight domain wall. (a) The lattice of xenon atoms with respect to the graphite. (b) The main and satellite Bragg scattering points in reciprocal space. The arrows indicate the directions of the scans shown in Fig. 9.

of a Lorentzian $1/[(Q-Q_0^2)^2+\kappa^2]$, to which we fit the longitudinal peak of the incommensurate phase. We only show the width of the incommensurate phase in the heating cycle.

One might speculate that this broadening results from a spread in the phase transition temperature across the sample. With this assumption we can estimate the longitudinal width

$$\Delta Q=\frac{\partial\epsilon}{\partial T}\Delta T=\frac{A}{3}\frac{1}{T_0^{\beta}}(T-T_0)^{\beta-1}\Delta T\ . \tag{5}$$

The solid line shown in the $\kappa$ versus $T$ plot [illustrated in Fig. 8(b)] is the above function with $\beta=\frac{1}{3}$, $T_0$ given from the fit to $\epsilon$ versus $T$, and a $\Delta T$ of 0.4 K. The general agreement is good except very close to the transition. It should be noted however that the $\kappa$ versus $\epsilon$ curve in Fig. 8(a) implies a power law $\kappa\propto\epsilon^{\alpha}$ with $\alpha=-2.6$, whereas Eq. (5) implies that $\alpha=-2$. It is interesting to speculate that the broadening shown in Fig. 7 may have an intrinsic origin as in, for example, the transition from the C phase to a reentrant fluid phase.[17,19,20] However, given the other potential sources for line broadening, the possibility that the weakly incommensurate phase is actually a highly correlated fluid could not be checked.

Villian[16] pointed out that the C-IC transition will be first order due to the effective attraction between walls

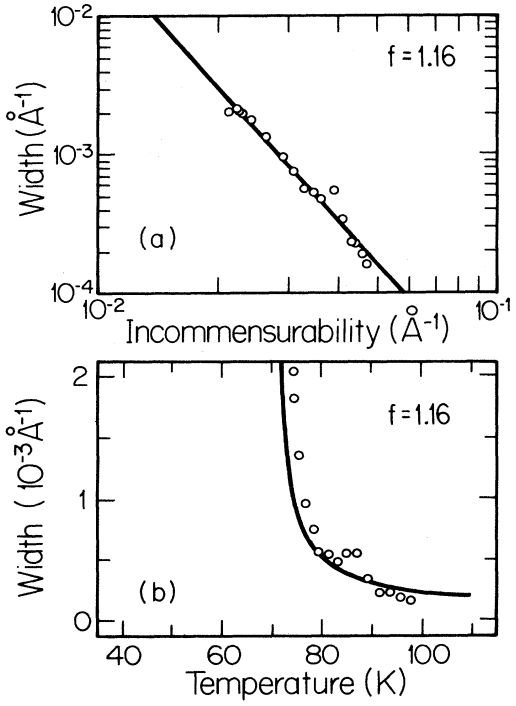


FIG. 8. Evolution of the measured longitudinal width near the C-IC transition. The line in (a) is a power law $K\sim\epsilon^{-\alpha}$ with $\alpha=-2.6$. The line in (b) is a power law with $\alpha=-2$ as discussed in the text.

caused by the entropic contribution of the breathing mode. According to mean-field theories[15] incorporating this feature, the C-IC transition from a hexagonal domain occurs for $l_c = \bar{a}e^{(1+2f_I/T)}$ [see Eq. (3)]. For the coverage of $f = 1.16$, the C-IC transition occurs at $l = 33a$ and $T \simeq 73$ K. Here $a$ is the lattice constant of the commensurate phase and $a/e < \bar{a} < 2a$. From this information we can estimate that $f_I$ is around 60 K assuming $\bar{a} \sim a$. This positivity of the wall crossing energy is predicted by Bak[36] and Talapov.[37] We will come back to this issue when we discuss the striped phase later.

In conclusion, the C-IC transition of the xenon monolayer, for coverages above one monolayer, is weakly first order, with behavior dominated by the breathing modes of hexagonal domains. The monolayer C-IC transition line terminates at 72.8 K, somewhat higher than the value of 62.5 K inferred by Hamichi *et al.*[31] However, there is no explicit contradiction between their data and ours as emphasized by them.[31]

Our data at 55 K are too sparse to allow a statement about the order of the transition. From their THEED experiments, Hamichi *et al.*[31] conclude that the C-IC transition at temperatures below $\sim 63$ K is continuous. We do not have measurements which contradict this result. However, given that the transition is first order at higher temperatures, a crossover to continuous behavior at lower temperatures would be quite surprising. We believe that kinetic issues in the THEED experiments need to be addressed carefully before this result can be considered to be established definitively.

### C. Hexagonal domain walls

Because the average lattice constant of a xenon incommensurate layer is larger than that of the commensurate phase, the domain walls of the xenon layer should either be *light* walls or *superlight* walls. Both the domain formation energy and the chemical potential deficiency prefer superlight walls. In Fig. 7(a) a network of superlight domain walls is illustrated. This network should lead to diffraction peaks at $(Q_{\text{comm}}, \epsilon)$ and $(Q_{\text{comm}} + \epsilon, -\epsilon)$ as illustrated in Fig. 7(b). We have taken the longitudinal and angular scans along the paths indicated in Fig. 7(b). The results shown in Figs. 9(a) and 9(b) are consistent with scattering from superlight walls. The satellites were only observed in the aligned incommensurate phase at low temperature. This does not, however, rule out the existence of hexagonal domain walls at higher temperatures.

We tabulate all of the reliable satellite intensities in Table I. Also tabulated are the data from the experiment using the vermicular graphite in the same sample cell. Since the intensities of the satellites for the data from the vermicular experiment are the sums of two identical satellite peaks, we divided the observed intensity by two to obtain the correct ratio for the vermicular data. In the powder experiment we measure only the absolute value of the wave vector. The peaks occurred at $Q_{\text{comm}} - \epsilon$ and $Q_{\text{comm}} + \epsilon/2$ for the main peak and the satellite peak, respectively. As shown in Table I, with increasing incommensurability the relative intensity of satellites in general decreases. The smaller intensities result mostly from the smaller size of the domain with an almost constant width of domain wall. As stated earlier, at the C-IC transition the domain size was $\sim 33a$, measured along a side of the hexagon; this is calculated directly from the incommensurability. The width of the domain wall was estimated to be $\sim 4a$ (half-width), which will be explained in Sec. IV D. The domain size decreases to $\sim 15a$ at the onset of the continuous rotation transition. When the domain size becomes smaller, more atoms sit inside the wall region. This further reduces the intensity of the satellites.

TABLE I. Estimation of domain-wall widths

| Coverage | $T$ (K) | $\epsilon$ | Ratio | Size | $l_0$ |
|---|---|---|---|---|---|
| | | Single-crystal data | | | |
| 0.96 | 61.34 | 0.0181 | 4.4 | 31 | 37.1 |
| 1.11 | 74.18 | 0.0265 | 13.9 | 22 | 48.2 |
| 1.02 | 71.27 | 0.0201 | 5.67 | 28 | 39.5 |
| 1.16 | 73.17 | 0.0205 | 7.2 | 27 | 43.7 |
| 1.16 | 76.97 | 0.0284 | 11.8 | 20 | 41.0 |
| 1.16 | 85.08 | 0.0385 | 15.2 | 14 | 31.9 |
| | | Vermicular data | | | |
| 1.16 | 81.5 | 0.0304 | 20.06 | 16 | 40.4 |
| | 81 | 0.0296 | 14.7 | 19 | 42.6 |
| | 74.51 | 0.0298 | 13.28 | 19 | 40.8 |
| | 72.25 | 0.0229 | 12.84 | 24 | 51.9 |

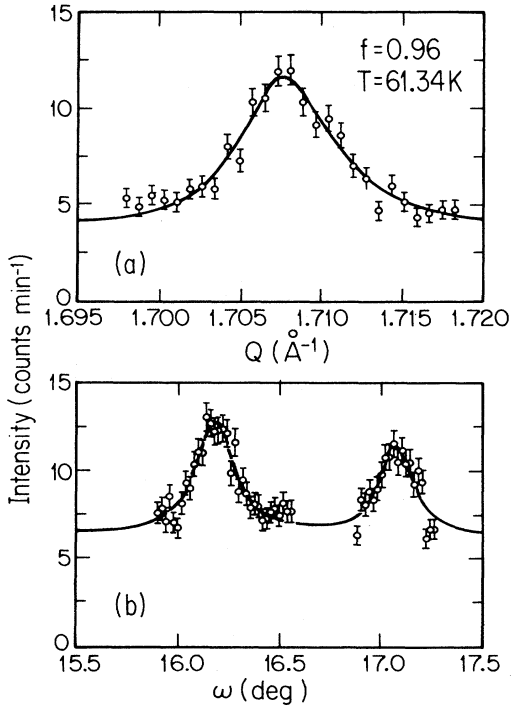


FIG. 9. Scans of the satellite peaks. Top: A longitudinal scan through the satellite as illustrated in Fig. 7(b). Bottom: An angular scan through the two satellites as illustrated in Fig. 7(b).

As a result, no satellites could be observed in the rotated incommensurate phase.

### D. Corrugation of the surface potential

The most reliable method for estimating the corrugation of the potential due to the substrate is to measure the domain-wall width. We assume that the meandering of walls does not significantly affect the intensities. The wall width then determines the ratio of intensities between the main peak and the satellite peaks. One can express the effective modulation of the adsorption potential for an adatom over the graphite surface as

$$V(\mathbf{r}) = -V_0[\cos(\mathbf{a}_1\cdot\mathbf{r})+\cos(\mathbf{a}_2\cdot\mathbf{r})+\cos(\mathbf{a}_3\cdot\mathbf{r})] , \quad (6)$$

where $\mathbf{a}_{1,2,3}$ are the reciprocal lattice vectors of the surface. The energy difference for a xenon atom between the center of a honeycomb and just above a carbon atom is $9/2V_0$. In Shiba's notation[23,24] the dimensionless wall width is $l_0=\sqrt{54W/V_0}$, where $W$ is the depth of the potential well between xenon atoms. The magnitude of $W$ is well established. Shiba's wall width $l_0$ is related roughly to the half-width at half maximum of the wall, $w$, by $l_0=10w$.

To compare theory with experiment we carried out a computer simulation for the domain-wall relaxation at zero temperature following Specht *et al.*[19] We varied $V_0$ until the resulting relaxation gave the right intensity of the satellite peak for each domain size. In this way we determined the $l_0$'s; they are also shown in Table I. Combining all of the data, the average $l_0$ is $41.7\pm5.5$. If we take only the single crystal data into consideration, $l_0$ becomes $40.2\pm5.6$. Considering the large variation in temperature and incommensurability, the consistency of the value of $l_0$ is quite satisfactory. This justifies the assumption that the thermal fluctuations do not significantly change the intensity ratio. By way of comparison, Shiba's $T=0$ theory[23,24] for the onset point of the xenon rotational transition yields $l_0=36$.

It is useful to compare the experimental value of $l_0$ with first-principle calculations of the xenon-graphite interaction potential. Steele[38] was the first to recognize the fact that we can approximate the lateral variation of the adsorption potential well using only the first Fourier components as in Eq. (6). Using the Lennard-Jones form of the potential between carbon and xenon, he calculated that the corrugation potential $9/2V_0$ should be 38.2 K. The most recent value for the potential depth resulting from the xenon-xenon interaction, $W$, is 282 K (Barker *et al.*[39]); this results in $l_0\simeq42.4$. Recently, Vidali and Cole[40] have reestimated the corrugation. Assuming no anisotropy in the xenon-carbon interaction they estimate $9/2V_0=77$ K, giving $l_0\simeq30$. Our estimation from the satellite intensities gives a value of $V_0$ closer to Steele's value. Halpin-Healy *et al.*[18] found that $9/2V_0=75$ K fits their proposed phase diagram best. They used $W=236$ K chosen by Rauber *et al.*[41] which together with their value for $9/2V_0$ gives $l_0\simeq27.7$.

The ratio of intensities of the main peak and satellite is independent of the thermal fluctuations to first order; however, we suspect that the intensity ratio yields an upper bound for $l_0$. This is because temperature effects should suppress the modulation.

Shiba's $l_0$ does not give the width of the walls directly. Instead of using the analytical function of the uniaxial pseudo-harmonic calculation by Villian[22] or the one by Bak[36] to estimate the width, we used directly the results of our relaxation simulation. The simulation produced the displacements from the commensurate site such that the resultant structure factor gave the correct ratio of scattering intensities. We found that a hyperbolic function fitted the calculated displacement profiles quite well. The function fitted to the displacements along one of the symmetry axes is

$$D = A\left[1-\tanh\left[\frac{n-C}{\lambda}\right]\right] , \quad (7)$$

where $A$ is 1.42 Å, $C$ is the size of the domain, and $n$ is the number for the row of atoms measured horizontally in Fig. 9(a). When $l_0$ is 40.4 and the size is $33a$, the $1/e$ full width is 7.1 rows. The displacements also fit quite well to the one dimensional Frank–van de Merwe theory,

$$D = A'\arctan(e^{n-c/\lambda}) . \quad (8)$$

With the same size, the fit for $\lambda$ gives 4.2. The pseudoharmonic results[22,36] $D=B\sinh[(n-C)/\lambda]$ do not fit well to our numerical simulations. From the above two functional forms, we can conclude that the half-width of the domain walls is approximately four rows of atoms.

### E. Vermicular data

As a consistency check we also performed an x-ray scattering experiment from a xenon layer adsorbed on to the vermicular graphite. There were two reasons for doing this part of the experiment. First, we wanted to check the equality of coverages on both types of graphite. Second, we intended to repeat the original Hong *et al.*[11] experiment with much higher resolution and thereby examine the proposed existence of the striped phase around a coverage of $f=1$ ML on vermicular graphite. The coherence length of the surface of vermicular graphite was $\sim700$ Å. This coherence length would always impose a peak wider than that of the resolution function in this experiment. On the other hand, Hong *et al.*'s previous experiment[11] had resolution-limited peaks.

Figure 10 shows scans from the vermicular experiment together with longitudinal and transverse scans from the single-crystal experiment at comparable temperatures. The vermicular scans were fitted to Warren's powder line shape averaged over a uniform mosaic distribution. Due to the mosiac distribution, one cannot see any of the angular features appearing in the single crystal experiment. We find generally that the reciprocal lattice vector $Q$ for the xenon on the vermicular graphite is the same, within errors, as the one obtained using the single-crystal substrate. This verifies that the coverages on the two substrates are identical, hence validating our experimental technique for controlling coverage on the single crystal.

However, in contrast to the single-crystal experiment,

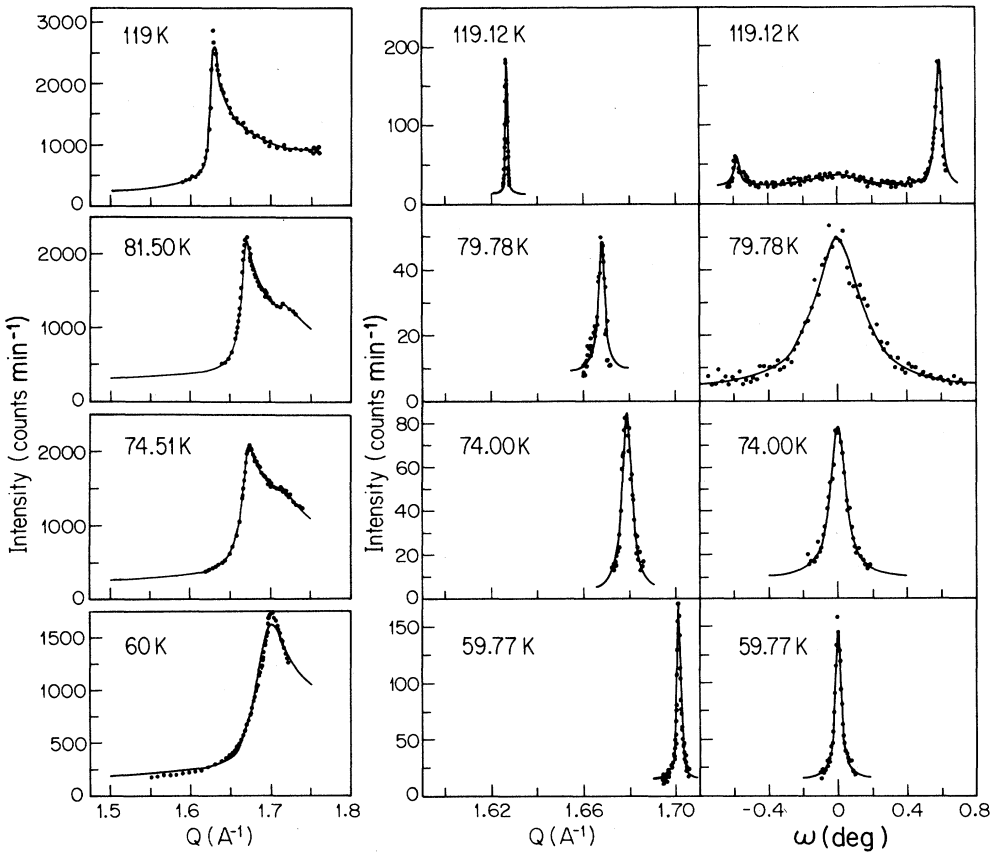


FIG. 10. Comparison of vermicular and single-crystal graphite substrate data. Representative scans for $f = 1.16$ layers of xenon on vermicular graphite compared with radial and angular scans for the same coverage on the KISH single-crystal graphite at comparable temperatures.

the commensurate phase does not readily appear in the vermicular experiment. This was already observed in Hong *et al.*'s previous experiment.[11] We did not see the two distinctive peaks indicating a striped phase as conjecture by Hong *et al.*[11] Instead, the peaks below 60 K are wide and cannot be fitted to a single peak. We could not deduce an ideal function for these peaks. However, an asymmetric distribution of reciprocal lattice vectors fits the data quite adequately. The fitting for the vermicular data at 60 K in Fig. 10 represents a triangular distribution of reciprocal lattice vectors with a cutoff at $Q_c$. This suggests that the low-temperature phase of xenon on the vermicular graphite is a pinned hexagonal domain-wall phase rather than a striped phase. This pinned hexagonal domain-wall phase may occur due to the defects on the surface including the edges and steps.[42,43]

## V. CONCLUSIONS

These experiments have clarified the phases and the phase transitions for a xenon solid layer on graphite in the monolayer coverage regime. The incommensurate solid undergoes the sequence of transitions: aligned→rotated→reentrant aligned, before the solid transforms into the commensurate solid. The current theory of orientational epitaxy correctly predicts only the point at which the rotation to the reentrant aligned phases occurs. None of the current theories can explain the whole picture of orientational epitaxy. Neither the high temperature aligned solid nor the reduction of the rotation angle from that of the static prediction are explained.

The reentrant aligned phase at low temperatures is an incommensurate solid with a network of superlight domain walls. The observed first-order phase transition can be explained within the domain-wall theory. The incommensurability at constant coverage decreases approximately as $[(T-T_0)/T_0]^{1/3}$ until the first order C-IC transition point is hit. This $\frac{1}{3}$ power law is close to the behavior seen for Kr on graphite following a similar thermodynamic pathway.[19]

We estimated the potential corrugation of the surface adsorption from the intensity ratios between the main and satellite peaks in the domain-wall incommensurate phase. The corrugation of the potential estimated was

close to the one predicted by Steele.[38] Along with the estimation from the onset of the rotated phase, we set the limits for the dimensionless wall width, $36 < l_0 < 42$.

At low temperatures the xenon layer on vermicular graphite did not transform into the commensurate phase as on the single-crystal graphite substrate. Instead the xenon layer seems to have a pinned domain-wall network due to defects.


## ACKNOWLEDGMENTS

We would like to thank T. Halpin-Healy, M. Kardar, and E. D. Specht for valuable discussions of these results. We are also grateful to J. A. Venables for copies of his work prior to publication and for stimulating comments. The work at MIT was supported by the Joint Services Electronics Program under Contract No. DAAL03-86-K-0002.



[1]P. Bak, Rep. Prog. Phys. **45**, 587 (1982).

[2]D. E. Moncton, J. D. Axe, and F. J. Disalvo, Phys. Rev. Lett. **34**, 734 (1975).

[3]R. J. Birgeneau and P. M. Horn, Science **232**, 329 (1986).

[4]P. Fischer, B. Lebech, G. Meier, B. D. Rainford, and O. Vogt, J. Phys. C **11**, 345 (1978).

[5]M. Kardar and A. N. Berker, Phys. Rev. Lett. **48**, 1552 (1982).

[6]R. G. Caflish, A. N. Berker, and M. Kardar, Phys. Rev. B **31**, 4527 (1985).

[7]B. Joos, B. Bergerson, and M. L. Klein, Phys. Rev. B **28**, 7219 (1983).

[8]B. Joos and M. S. Duesbery, Phys. Rev. B **33**, 8632 (1986).

[9]K. L. D'Amico and D. E. Moncton, J. Vac. Sci. Technol. A **4**, 1455 (1986).

[10]P. S. Schabes-Retchman and J. A. Venables, Surf. Sci. **105**, 536 (1981).

[11]H. Hong, R. J. Birgeneau, and M. Sutton, Phys. Rev. B **33**, 3344 (1986).

[12]H. Hong, C. J. Peters, A. Mak, R. J. Birgeneau, P. M. Horn, and H. Suematsu, Phys. Rev. B **36**, 7311 (1987).

[13]W. L. McMillan, Phys. Rev. B **14**, 1496 (1976).

[14]F. C. Frank and J. H. van der Merwe, Proc. R. Soc. London, Ser. A **198**, 205 (1949).

[15]S. N. Coppersmith, Daniel S. Fisher, B. I. Halperin, P. A. Lee, and W. F. Brinkman, Phys. Rev. B **25**, 349 (1982).

[16]J. Villian, in *Ordering in Strongly Fluctuating Condensed Matter Systems,* edited by T. Riste (Plenum, New York, 1980).

[17]S. N. Coppersmith, D. S. Fisher, B. I. Halperin, P. A. Lee, and W. F. Brinkman, Phys. Rev. Lett. **46**, 549 (1981).

[18]T. Halpin-Healy and M. Kardar, Phys. Rev. B **34**, 6557 (1986).

[19]D. E. Moncton, P. W. Stephens, R. J. Birgeneau, P. M. Horn, and G. S. Brown, Phys. Rev. Lett. **46**, 1533 (1981); E. D. Specht, A. Mak, C. J. Peters, M. Sutton, R. J. Birgeneau, K. L. D'Amico, D. E. Moncton, S. E. Nagler and P. M. Horn, Z. Phys. B **69**, 347 (1987).

[20]J. Lui, S. C. Fain, Jr., H. Freimuth, H. Weichert, H. P. Schildberg, and H. J. Lauter, Phys. Rev. Lett. **60**, 1848 (1988).

[21]A. D. Novaco and J. P. Mctague, Phys. Rev. Lett. **38**, 1286 (1977).

[22]J. Villian, Phys. Rev. Lett. **41**, 36 (1978).

[23]H. Shiba, J. Phys. Soc. Jpn. **46**, 1852 (1979).

[24]H. Shiba, J. Phys. Soc. Jpn. **48**, 211 (1980).

[25]T. Halpin-Healy, Ph.D. thesis, Harvard University, 1987.

[26]A. Thomy, J. Reginier, J. Menaucourt, and X. Duval, J. Cryst. Growth. **13/14**, 159 (1972).

[27]P. A. Heiney, P. W. Stephens, R. J. Birgeneau, P. M. Horn, and D. E. Moncton, Phys. Rev. B **28**, 6416 (1983).

[28]P. Dimon, P. M. Horn, M. Sutton, R. J. Birgeneau, and D. E. Moncton, Phys. Rev. B **31**, 437 (1985).

[29]C. G. Shaw, S. C. Fain, Jr., and M. C. Chinn, Phys. Rev. Lett. **41**, 955 (1978).

[30]K. L. D'Amico, D. E. Moncton, E. D. Specht, R. J. Birgeneau, S. E. Nagler, and P. M. Horn, Phys. Rev. Lett. **53**, 2250 (1984).

[31]A. Q. D. Faisal, M. Hamichi, G. Raynerd, and J. A. Venables, Phys. Rev. B **34**, 7440 (1986). For recent THEED work see M. Hamichi, A. Q. D. Faisal, J. A. Venables, and R. Kariotis, Phys. Rev. B **39**, 415 (1989).

[32]C. W. Mowforth, T. Rayment, and R. F. Thomas, J. Chem. Soc. Faraday Trans 2 **82**, 1621 (1986).

[33]P. W. Stephens, P. A. Heiney, R. J. Birgeneau, P. M. Horn, D. E. Moncton, and G. S. Brown, Phys. Rev. B **29**, 3512 (1984).

[34]S. C. Fain, Jr., M. D. Chinn, and R. D. Diehl, Phys. Rev. B **21**, 4170 (1980).

[35]V. L. Pokrovsky and A. L. Talapov, Phys. Rev. Lett. **42**, 65 (1979).

[36]P. Bak, in *Solitons and Condensed Matter Physics,* edited by A. R. Bishop and T. Schneider (Springer-Verlag, Berlin, 1978).

[37]A. L. Talapov, Phys. Rev. B **24**, 6703 (1981).

[38]W. A. Steele, Surf. Sci. **36**, 317 (1973).

[39]J. A. Barker, M. L. Klein, and M. V. Bobetic, IBM J. Res. Develop. **20**, 222 (1976).

[40]G. Vadali and M. W. Cole, Phys. Rev. B **29**, 6736 (1984).

[41]S. Rauber, J. R. Klein, and M. W. Cole, Phys. Rev. B **27**, 1314 (1983).

[42]J. Villian, J. Phys. Lett. (Paris) **41**, L267 (1980).

[43]J. Villian and M. B. Gordon, in *Dynamical Processes and Ordering on Solid Surfaces,* Vol. 59 of *Springer Series in Solid-State Sciences,* edited by A. Yoshimori and M. Tsukada, (Springer, Berlin, 1985), p. 144.